ISSN 1027-5495. Functional Materials, 27, No.4 (2020), p. 687-694.
doi:https://doi.org/10.15407/fm27.04.687 

# The effect of heat treatment on the magnetic properties of ZnO:Mn nanocrystals obtained by ultrasonic aerosol pyrolysis

***O.V.Kovalenko, V.Yu.Vorovsky, O.V.Khmelenko***

O.Honchar Dnipro National University, 72 Gagarin Ave.,
49010 Dnipro, Ukraine

*Received April 1, 2020*

Samples of ZnO:Mn nanocrystals (impurity concentration 2 at.%) were obtained by ultrasonic aerosol pyrolysis and subjected to heat treatment in air at temperatures of 550°C and 850°C, as well as in a gas medium with hydrogen at a temperature of 550°C. The term of the heat treatment was 20 min. The nanocrystal samples were cooled in a flow of nitrogen gas for 15 min. The samples were studied by X-ray phase analysis, EPR, and the magnetic vibration method before and after annealing. The synthesized samples had ferromagnetic properties at room temperature. The specific magnetization of the sample was $M_s$ = 0.028 emu/g. Heat treatment at $T$ = 550°C led to a decrease in the specific magnetization of the samples ($M_s$ = 0.01 emu/g). After heat treatment at $T$ = 850°C, the ferromagnetic properties in the samples disappeared. Ferromagnetic properties of the samples were restored after heat treatment in a gas medium with hydrogen ($M_s$ = 0.023 emu/g). The regularities of the influence of heat treatment regimes on the magnetic properties of ZnO:Mn nanocrystals are explained by a change in both the number and the ratio of intrinsic defects (oxygen vacancies $V_O$) and impurity $Mn^{2+}$ ions located in the surface layer of nanocrystals.

**Keywords**: nanocrystals, zinc oxide, heat treatment in air, heat treatment in a hydrogen atmosphere, ferromagnetic properties, X-ray phase analysis, EPR spectra, intrinsic defects, impurity defects.

**Вплив режимів термічної обробки на магнітні властивості нанокристалів ZnO:Mn, отриманих методом ультразвукового піролізу аерозоля**. *О.В.Коваленко, В.Ю.Воровський, О.В.Хмеленко.*

Зразки нанокристалів ZnO:Mn (концентрація домішки 2 ат.%) отримано методом ультразвукового піролізу аерозоля та підлягалися термічній обробці на повітрі при температурах 550°C та 850°C, а також у газовому середовищі з воднем при температурі 550°C. Термін термічної обробки дорівнював 20 хв. Охолодження зразків нанокристалів проводилося у потоці газоподібного азоту протягом 15 хв. Зразки до та після відпалу досліджувалися методами рентгено-фазового аналізу, ЕПР та магнітовібраційним методом. Синтезовані зразки мали феромагнітні властивості при кімнатній температурі. Питома намагніченність зразка складає $M_s$ = 0,028 Гс·см$^3$/г. Термічна обробка при $T$ = 550°C приводила до зменшення питомої намагніченості зразків ($M_s$ = 0,01 Гс·см$^3$/г). Під час термічної обробки при $T$ = 850°C феромагнітні властивості у зразків зникають і відновлюються після термічної обробки у газовому середовищі з воднем ($M_s$ = 0,023 Гс·см$^3$/г). Такі закономірності впливу режимів термічної обробки на магнітні властивості зразків нанокристалів ZnO:Mn пояснюються зміною як кількості, так і співвідношенням власних (вакансії кисню Vo) та домішкових (іони $Mn^{2+}$) дефектів, розташованих у приповерхневому шарі нанокристалів.

Образцы нанокристаллов ZnO:Mn (концентрация примеси 2 at.%) получены методом ультразвукового пиролиза аэрозоля и подлежали термической обработке на воздухе при температурах 550°C и 850°C, а также в газовой среде с водородом при температуре 550°C. Срок термической обработки равен 20 мин. Охлаждение образцов нанокристаллов проводилось в потоке газообразного азота в течение 15 мин. Образцы до и после отжига исследовались методами рентгено-фазового анализа, ЭПР и магнито-вибрационным методом. Синтезированные образцы имели ферромагнитные свойства при комнатной температуре. Удельная намагниченность образца составляет $M_s$ = 0,028 Гс·см$^3$/г. Термическая обработка при $T$ = 550°C приводит к уменьшению удельной намагниченности образцов ($M_s$ = 0,01 Гс·см$^3$/г). Во время термической обработки при $T$ = 850°C ферромагнитные свойства в образцах исчезают и восстанавливаются после термической обработки образцов в газовой среде с водородом ($M_s$ = 0,023 Гс·см$^3$/г). Такие закономерности влияния режимов термической обработки на магнитные свойства образцов нанокристаллов ZnO:Mn объясняются как изменением количества, так и соотношением собственных (вакансии кислорода Vo) и примесных (ионы $Mn^{2+}$) дефектов, размещенных в приповерхностном слое нанокристаллов.

## *1. Introduction*

Diluted magnetic semiconductors (DMS) are in the spotlight of researchers because of their potential for use in various spintronic devices [1, 2]. In recent years, significant successes have been achieved in the development of synthesis methods of DMS which have ferromagnetic properties (FP) at room temperature. The theoretical foundations of ferromagnetism in ZnO based DMS doped with Mn were developed in [3]. Further intensive experimental studies showed that the FP of such materials substantially depends on the technological conditions of production. They acquire FP during low-temperature synthesis ($T_c$ < 500°C) with low concentrations of the manganese dopant (Mn < 4 at. %) [4]. Also, the influence of heat treatment on the FP of samples was noted. It was found in [5] that samples synthesized by the solid-phase method at $T_c$ = 500°C showed FP, but heat treatment at $T$ > 700°C leads to a decrease, and annealing at $T$ > 900°C leads to complete loss of FP. In other works, it was found that the conditions in which the samples are heat treated are important. So, it was shown in [6] that annealing of samples in vacuum or in $N_2$ atmosphere leads to the appearance of FPs, and thermal treatment in $O_2$ atmosphere leads to their disappearance. It was shown in [7] that heat treatment of samples in a hydrogen atmosphere can transform them from a paramagnetic to a ferromagnetic state. Such processing can also restore the FP lost during the annealing of the samples at 800°C.

The above results indicate the decisive role of crystal lattice defects in the formation of the FP of the DMS. According to the model of bound magnetic polaron (BMP) [8, 9], FP in ZnO:Mn nanocrystals (NCs) are due to the exchange interaction between $Mn^{2+}$ ions indirectly through intrinsic defects of the crystal lattice. This is confirmed by the results of [10]. In this case, intrinsic defects, for example, oxygen vacancies (Vo), act as intermediaries in the exchange interaction between the $Mn^{2+}$ impurity defects. The condition of ferromagnetic ordering in the NCs of DMS is not only the presence, but also the corresponding structure of intrinsic defects [10, 11]. It was shown that such a structure of defects can be formed by mechanical grinding of ZnO:Mn polycrystals in an inert medium [12]. With such mechanical treatment, a defective surface layer with a large number of oxygen vacancies (Vo) is formed in the NC. This creates the conditions for the interaction of $Mn^{2+}$ impurity ions with each other using Vo as an intermediate link and leads to the appearance of FP in ZnO:Mn samples at room temperature.

A similar defect structure which leads to the appearance of FP, was created in ZnO:Mn nanocrystals after their synthesis by ultrasonic aerosol pyrolysis (UAP) [13]. The peculiarity of the formation of NCs during this synthesis determines the presence of a large number of defects and the existence of an inhomogeneous crystalline structure in the form of a defect-free core and a defective shell [14].

Thus, the study of the role of temperature conditions for the synthesis of DMS and the conditions of heat treatment of the obtained samples is an urgent task. Such studies make it possible to develop methods for the synthesis of DMS with FP, as well as to answer the question of the role of intrinsic and impurity defects in the forma-

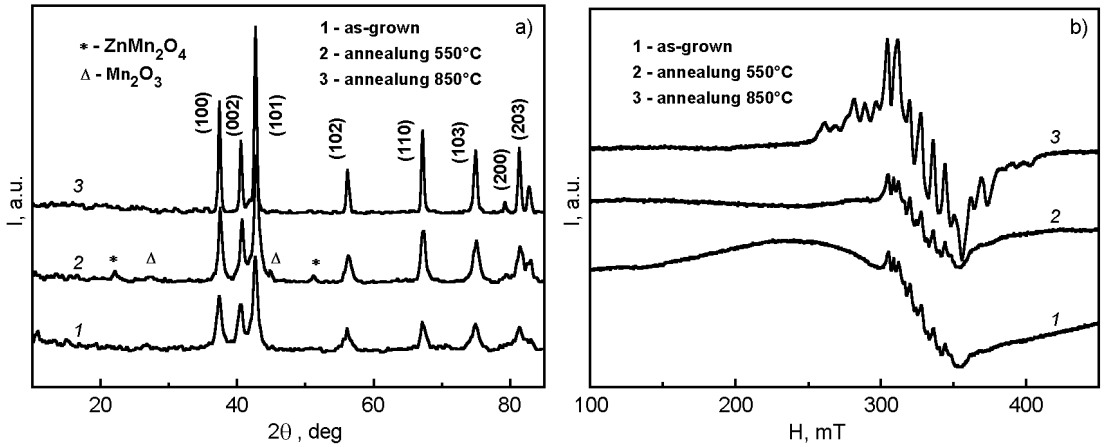


Fig. 1. X-ray powder diffraction data (a) and EPR spectra (b) of nanocrystals ZnO:Mn (2 at.%): *1* — before annealing in air; *2* — after annealing at $T$ = 550°C; *3* — after annealing at $T$ = 850°C. The symbols * and Δ denote the impurity phases $ZnMn_2O_4$ and $Mn_2O_3$, respectively.

tion of FP. The aim of this work is to establish the effect of heat treatment on the structure of defects and the magnetic characteristics of ZnO:Mn nanocrystals obtained by the UPA method.

## 2. Experimenal

The UPA method is based on the thermal decomposition of aerosol droplets of a solution of the starting components during their passage through the thermal zone of the furnace [15]. In this method, it is possible to control the following parameters of the final product: the size of NCs, and the defectiveness of their surface. This method also allows alloying of NCs with various impurities. The main feature of UPA method for the NC synthesis is that the NCs form as micro-droplets in the bulk under nonequilibrium conditions, which, in turn, leads to the appearance of a large number of defects in the NCs.

We synthesized samples of ZnO:Mn nanocrystals with a manganese concentration of 2 at.% according to the method described in [13]. For the synthesis, aqueous solutions of zinc and manganese nitrates were used. The synthesis occurred at a temperature $T_s$ = 550°C. The obtained samples were annealed in air at temperatures of 550°C and 850°C. In addition, they were heat treated in a flow of a mixture of hydrogen and nitrogen gases in the ratio $H_2/N_2$ ~ 1/3 at a temperature of 550°C. In order to prevent an increase in the dimensions of NCs, the heat treatment regime was short-term; it lasted for 20 min. In this case, the samples were cooled in the cold zone of the furnace for 15 min in a flow of gaseous nitrogen.

The crystal structure and phase composition of the samples were studied by X-ray phase analysis (XRD) on a DRON-2 diffractometer using CoKα radiation (λ = 1.7902 Å), EPR studies of the samples were carried out on a RADIOPAN SE/X 2543 radio spectrometer. The magnetic properties of the samples were studied by vibromagnetometry.

## 3. Results and discussion

The results of studying the crystal structure and phase composition of ZnO:Mn nanocrystals samples are shown in Fig. 1. It was shown that the crystal structure of ZnO:Mn nanocrystals is a hexagonal wurtzite type. The average sizes of ZnO:Mn nanocrystals were calculated using the Scherrer formula [16]. The results of calculations of the crystal lattice parameters ($a$ and $c$), unit cell volume ($V$), and average NC size ($d$) are given in Table. From these data it follows that the lattice parameters $a$ and $c$ in ZnO:Mn nanocrystals are much smaller than in single-crystal ZnO [17]. This is explained by the nonequilibrium conditions of the crystallization of nanocrystals, which determine the presence of deformation stresses in the crystal lattice of ZnO nanocrystals.

With an increase in the annealing temperature of the samples, the amplitudes increase and the widths of reflections in the X-ray diffraction patterns decrease (Fig. 1a). Such changes are a consequence of an increase in the size of NCs and an approximation of the crystal lattice parameters of ZnO:Mn nanocrystals to the parame-

Table. Parameters of the crystal lattice, unit cell volume, and average size of ZnO:Mn nanocrystals

| | $a$, Å | $c$, Å | $V$, Å$^3$ | $d$, nm |
|---|---|---|---|---|
| Synthesized | 3.2396 | 5.1873 | 47.145 | 34.9 |
| After annealing at $T$ = 550°C | 3.2397 | 5.1871 | 47.146 | 36.2 |
| After annealing at $T$ = 850°C | 3.2403 | 5.1923 | 47.211 | 63.7 |
| ZnO single crystal [17] | 3.2492 | 5.2053 | 47.589 | – |

ters of bulk crystals (Table). qAnalysis of the XRD data shows that the phase composition of the synthesized sample before annealing is homogeneous and corresponds to the chemical compound ZnO. After annealing at a temperature of 550°C, impurity phases $Mn_2O_3$ and $ZnMn_2O_4$ appear in the sample, which disappear after heat treatment at 850°C.

This fact may indicate that in the synthesized ZnO:Mn nanocrystal sample, there is an intercrystalline medium in which the Mn impurity can be concentrated in the form of amorphous clusters or small nuclei of impurity phases. These inclusions are not detected by XRD. During high-temperature annealing, an intense process of doping ZnO nanocrystals with the Mn impurity occurs due to the decomposition of the impurity phases $Mn_2O_3$ and $ZnMn_2O_4$. Short term annealing (20 min) does not lead to a significant increase in the size of the nanocrystals (Table). Thus, the results indicate that in the synthesized ZnO:Mn nanocrystals, the Mn impurity can be located in an amorphous intergranular medium. The crystal lattice of ZnO:Mn nanocrystals is strained.

The EPR spectra of ZnO:Mn nanocrystals before and after the heat treatment are shown in Fig. 1b. In these spectra, a hyperfine structure (HFS) is observed at the magnetic field $H$ = 325 mT. It consists of six lines and is associated with $Mn^{2+}$ ions located in the nodes of the ZnO crystal lattice. From the intensity of these lines, the concentration of $Mn^{2+}$ ions in ZnO:Mn nanocrystals can be obtained. It should be noted that the HFS lines in the EPR spectra are superimposed on a broad background absorption line, which is associated with the exchange interaction of $Mn^{2+}$ ions [18].

In the EPR spectrum of the sample prior to annealing (Fig. 1b, spectrum *1*), in addition to the HFS lines of $Mn^{2+}$ ions, a broad, nonstructural line located in a weak magnetic field $H$ ~ 250 mT ($g$ ~ 4.0) was also detected. This absorption line may indicate the presence of a large number of acceptor type defects in the sample. Also, this line can be associated with ferromagnetic resonance due to the presence of a ferromagnetic phase in the sample. According to [19], this phase arises as a result of an exchange interaction of $Mn^{2+}$ impurity ions with acceptor-type defects in the crystal lattice. The line of ferromagnetic resonance in the EPR spectra is a sign of the presence of ferromagnetism in the samples at room temperature. After annealing the nanocrystals at $T$ = 550°C and $T$ = 850°C, this line disappears due to a decrease in the number of intrinsic defects.

The heat treatment at $T$ = 550°C leads to a decrease in the background line intensity and a slight increase in the amplitudes of the lines of cold fusion of $Mn^{2+}$ ions (Fig. 1b, spectrum *2*). This is due to a decrease in the amount of $Mn^{2+}$ impurity ions that take part in the exchange interaction. During annealing, some of them begin to participate in the doping of ZnO nanocrystals, which, in turn, takes place in the lattice sites, and leads to an increase in the concentration of $Mn^{2+}$ ions in NCs. Another part of the impurity ions $Mn^{2+}$ participates in the formation of impurity phases $Mn_2O_3$ and $ZnMn_2O_4$. From this we can conclude that the doping of ZnO nanocrystals with $Mn^{2+}$ ions during short-term synthesis by the UPA method is particular. Thus, the obtained results indicate that in the samples prior to annealing, the distribution of the dopant Mn ions in the bulk of ZnO nanocrystals is inhomogeneous.

After annealing the sample at a temperature of 850°C in air, the shape of the EPR spectrum changed (Fig. 1b, spectrum *3*). The intensity of the HFS lines of $Mn^{2+}$ ions increases significantly, while the intensity of the broad background line decreases. This may indicate that, due to thermal diffusion, almost all Mn impurity ions are located at the sites of the ZnO crystal lattice. Thus, it can be argued that the distribution of the $Mn^{2+}$ dopant in the bulk of ZnO nanocrystals has become more uniform. This, in turn, leads to a significant decrease in the thickness of the defective surface

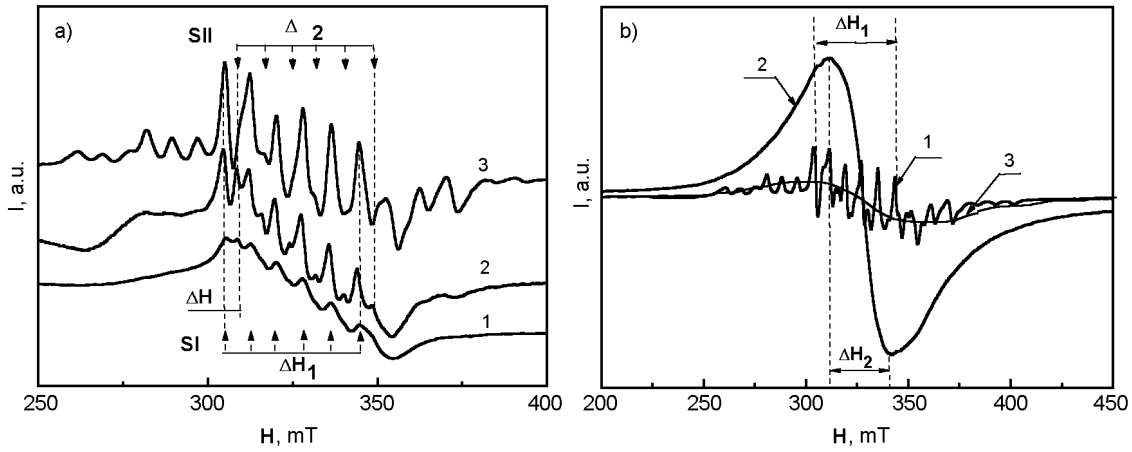


Fig. 2. EPR spectra (a) of a NC sample ZnO:Mn (2 at%): *1* — before annealing, *2* — after annealing at $T$ = 550°C, *3* — after annealing at $T$ = 850°C; EPR spectra (b) of this sample: *1* — after annealing at $T$ = 850°C; *2* — after annealing in a mixture of hydrogen and nitrogen gases in the ratio $H_2/N_2$ ~ 0.3; *3* — wide background absorption line due to the exchange interaction of impurities $Mn^{2+}$ ions.

layer. Long-term annealing of the sample leads to its complete disappearance. It should be emphasized that in the EPR spectra of ZnO:Mn nanocrystals, after annealing at $T$ = 850°C, additional low-intensity EPR lines appear on both sides of the HFS of $Mn^{2+}$ ions. Establishing their nature requires additional research.

It should be noted that after annealing at $T$ = 550°C, the HFS lines of $Mn^{2+}$ ions double in the EPR spectrum (Fig. 2a, spectrum *2*). This may be an additional evidence of the existence of a core-shell structure in the NC samples. The EPR spectrum in this case consists of a superposition of two spectra. The SI spectrum is caused by $Mn^{2+}$ ions, which replace $Zn^{2+}$ ions in the crystal lattice sites of ZnO nanocrystals. The SII spectrum is associated with $Mn^{2+}$ ions, which can be located in the strained surface layer, where local symmetry is excited around them. In [20] also came to this conclusion. Possibly during annealing, it is precisely on the surface of the NC that manganese compounds $Mn_2O_3$ and $ZnMn_2O_4$ are formed, in which $Mn^{2+}$ ions are in a different local environment. An analysis of the EPR spectra shows that the shift between the lines of the SI and SII spectra is $DN$ = 3.9 mT. The width of the SI line is $\Delta H_1$ = 39.52 mT, the hyperfine coupling constant $A_1$ = 7.90 mT. Such a value of the constant $A_1$ corresponds to the tetrahedral environment of $Mn^{2+}$ ions in the ZnO crystal lattice. The width of the SII line is $\Delta H_2$ = 39.85 mT, the constant $A_2$ = 7.96 mT. It can be assumed that $Mn^{2+}$ ions, which are located on the surface of nanocrystals, are also in tetrahedral surroundings.

The presence of a defective near-surface layer in ZnO:Mn nanocrystals is explained by the molecular-kinetic theory of their growth from a supersaturated solution [21]. According to this theory, the formation of NCs can be represented in three successive stages. Due to the short period of synthesis by the UPA method, the formation of ZnO:Mn nanocrystals is completed at the first stage — the appearance of the nuclei of NCs and their molecular diffusion growth. A feature of this stage is that the growth of the nuclei will occur over time from a more depleted solution. Under these conditions, the delivery of atoms to a growing surface is complicated. This causes the formation of NC with a perfect crystalline nucleus and a defective surface shell. It contains various types of intrinsic defects, such as interstitial zinc ($Zn_i$), interstitial oxygen ($O_i$), zinc and oxygen vacancies ($V_{Zn}$, $V_O$), as well as dopant ions $Mn^{2+}$. In this case, the dopant will be forced into this surface layer and be surrounded by structural defects [22].

As we indicated earlier, after annealing the sample in air at $T$ = 850°C, the near-surface layer disappears and the SII spectrum disappears too (Fig. 2a, spectrum *3*). This near-surface defective layer can be restored by modifying the surface of the NC, for example, by annealing in a hydrogen medium.

The EPR spectrum of the sample after heat treatment at $T$ = =550°C in a hydrogen atmosphere is shown in Fig. 2b (spec-

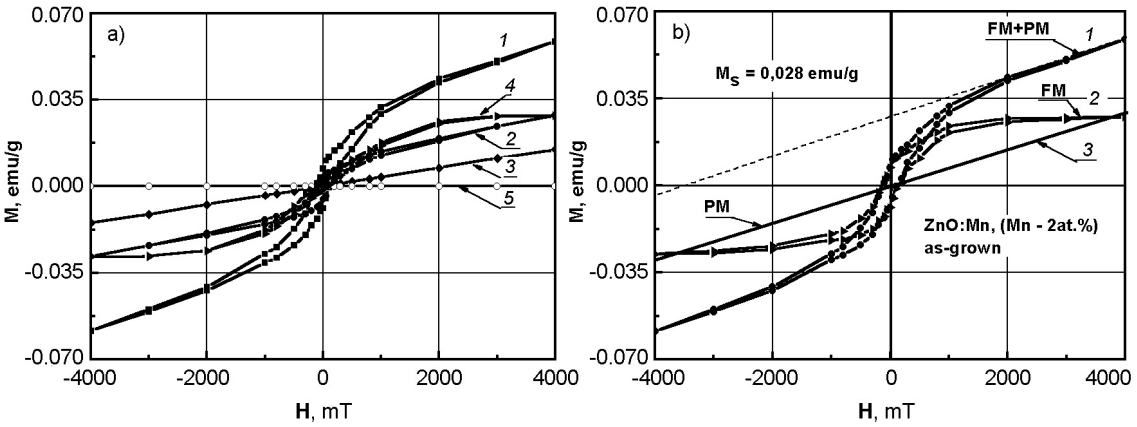


Fig. 3. Field dependent magnetization (a) of samples ZnO:Mn (2 at.%): *1* — synthesized, heat treated; *2* — after annealing at $T = 550$°C (20 min.); *3* — after annealing at $T = 850$°C (20 min.); *4* — after additional (20 min) annealing of sample (3) in a gas medium containing hydrogen (in the ratio $H_2/N_2 = 0.5$); *5* — after annealing in air at $T = 850$°C (1 h). Separation of the paramagnetic component (b) with the magnetization curve of the synthesized sample (sample 1): *1* — experimental curve; *2* — ferromagnetic component of the magnetization of the sample (FM); *3* — paramagnetic component (PM).

trum *2*). This sample was subjected to short-term annealing in air at $T = 850$°C. Its EPR spectrum is also shown in Fig. 2b (spectrum *1*), i.e. EPR spectra in Fig. 2a (spectrum *3*) and the EPR spectrum in Fig. 2b (spectrum *1*) are the same. As a result of heat treatment in a hydrogen atmosphere, the amplitude of the absorption line increases several times. This indicates a significant change in the defective near-surface state of the NC. The width of the EPR spectrum line decreases from $\Delta H_1 = 39.52$ mT to $\Delta H_2 = 29.10$ mT. In the ZnO semiconductor, hydrogen acts as a shallow donor ($H^+$) increasing the number of free electrons in the conduction band [23]. The action of hydrogen is caused its high reaction properties. It can form oxygen vacancies ($V_O$) and bind with intrinsic defects of nanocrystals and with dopant ions to form hydrogen complexes [24]. These complexes, as a rule, have unpaired electron spins and intrinsic magnetic moment. Therefore, the EPR spectra of these samples will have additional contributions due to the presence of free electrons and hydrogen complexes, which increase the intensity of the background.

The effect of heat treatment on the magnetic characteristics of ZnO:Mn samples (2 at.%) is shown in Fig. 3. The synthesized sample has the maximum magnetization value before annealing. Heat treatment at $T = 550$°C in air leads to a decrease in the magnetization of the samples. It should be noted that the magnetization curves of these samples do not have a saturation state. This indicates that in addition to the ferromagnetic component, there also exists a paramagnetic component. The amount of the paramagnetic phase is determined by the angle of inclination of the lines touching these curves. Taking into account the fact that the paramagnetic properties of the samples have a linear dependence on the magnetic field, when they disappear at a zero magnetic field, we can distinguish the ferromagnetic component from the experimental magnetization curves and determine the maximum specific magnetization of the samples in the saturation state $M_s$ (Fig. 3b). After the analysis, it was found that the specific magnetization of the sample during annealing has a value of $M_s = 0.028$ emu/g, and after annealing at $T = 550$°C this value decreases almost three times ($M_s = 0.01$ emu/g).

The sample was heat-treated in air at $T = 850$°C (20 min) and became completely paramagnetic (Fig. 3a, line *3*). After prolonged annealing of the sample for 1 h, it completely loses its magnetic properties (Fig. 3a, line *5*). It is interesting that annealing of this sample in a gas medium with hydrogen leads to the restoration of its ferromagnetic properties (Fig. 3b, line *4*). In this case, the magnetization curve has a saturation state. The specific magnetization of the sample in this case is $M_s = 0.023$ emu/g. The presence of the saturated state is a sign of the absence of a paramagnetic phase in the sample. Similar magnetization values ($M_s = 0.016$ emu/g) were obtained in

[25] after heat treatment of a paramagnetic ZnO powder doped with 2 at.% Mn in a hydrogen atmosphere at a temperature $T = 500$°C.

To explain the effect of heat treatment on the FP of nanocrystals, it is necessary to take into account the role of crystal lattice defects in their formation, as well as how the number and ratio of participants in the exchange interaction (intrinsic and impurity defects) change. These processes occur in the surface layer of the nanocrystal, and not in its crystalline core. Ions of the $Mn^{2+}$ impurity located at the sites of the ZnO crystal lattice and $Mn^{2+}$ ions causing the hyperfine structure lines in the EPR spectra, do not participate in the exchange interaction, and therefore do not affect the magnetic state of the samples. Separate impurity $Mn^{2+}$ ions located in the near-surface defective layer determine the paramagnetic properties. $Mn^{2+}$ ions located in the near-surface defective layer participate in the exchange interaction with the help of intrinsic defects and determine the FP of the nanocrystals [10, 26]. The presence of a significant amount of impurity ($Mn^{2+}$ ions) and intrinsic defects (oxygen vacancies, $V_0$) in the synthesized sample explains the maximum magnetization of the sample. After annealing in air at $T = 550$°C, the number of such defects decreases, which leads to a decrease in the magnetization of the sample. Oxygen vacancies $V_0$ completely disappear after short-term annealing of the sample (20 min) in air at a temperature of 850°C, which results in the disappearance of the FP of the sample. In this case, a certain amount of paramagnetic impurity $Mn^{2+}$ ions remains, which causes insignificant paramagnetic properties of the sample (Fig. 3a, line *3*). Long-term annealing for 1 h at $T = 850$°C leads to the disappearance of paramagnetic properties (Fig. 3, line *5*) because in this case all paramagnetic $Mn^{2+}$ ions take part in the doping of ZnO nanocrystals. The restoration of ferromagnetic properties after heat treatment of the sample in an atmosphere containing hydrogen occurs due to the appearance of a large number of intrinsic defects on the surface of nanocrystals, including oxygen vacancies $V_0$. The presence of these vacancies and impurity $Mn^{2+}$ ions remaining after a short-term annealing of the sample at $T = 850$°C, creates the conditions for the appearance of FP.

## *4. Conclusions*

It has been established that, during UPA synthesis, ZnO:Mn nanocrystals acquire a "core-shell" structure. They consist of a single-crystalline core and a defective surface layer. Such nanocrystals have ferromagnetic properties at room temperature. The maximum value of magnetization is $M_s = 0.028$ emu/g.

The effect of heat treatment on the defect structure and magnetic properties of ZnO:Mn nanocrystals has been determined. Heat treatment of the sample in air at $T = 550$°C (20 min) leads to a decrease in the magnetization of the samples to $M_s = 0.01$ emu/g. After heat treatment in air at $T = 850$°C (20 min), the sample loses FP and becomes paramagnetic. Prolonged annealing of the thread for 1 h leads to "falling asleep" of magnetic properties.

It is shown that the FP can be restored by heat treatment of samples in a hydrogen-containing gas medium. This fact is explained by the activity of hydrogen on the surface of NCs; as a result, NCs become structurally inhomogeneous.

It has been established that the FP of ZnO:Mn nanocrystals is affected both by the number and the ratio of exchange interaction participants — intrinsic (oxygen vacancies $V_0$) and impurity ($Mn^{2+}$ ions) defects located in the defective near-surface layer of the NC. Thus, the obtained experimental results are in qualitative agreement with the conclusions of the theoretical model of a coupled magnetic polaron, which explains the nature of the appearance of FP in the DMS.

## *References*


1. I.Zutic, J.Fabian, S.C.Erwin, *IBM J.Res. Dev.*, **50**, 121 (2006).
2. S.M.Pogorily, S.M.Ryabchenko, A.I.Tovstolitkin, *Ukr.J.Phys.Rev.*, **6**, 37 (2010).
3. T.Dietl, H.Ohno, F.Matsukura et al., *J.Science*, **287**, 1019 (2000).
4. J.Zhang, R.Skomski, D.J.Sellmyer, *J.Appl. Phys.*, **97**, 10D303 (2005).
5. P.Sharma, A.Gupta, K.Rao et al., *J.Nature Mater.*, **2**, 673 (2003).
6. D.Rubi, J.Fontcuberta, A.Calleja et al., *Phys. Rev. B*, **75**, 155322 (2007).
7. V.K.Sharma, G.D.Varma, *J.Appl.Phys.*, **102**, 056105 (2007).
8. J.M.D.Coey, M.Venkatesan, C.B.Fitzgerald, *J. Nature Mater.*, **4**, 173( 2005).
9. R.Mukherji, V.Mathur, *J.Nano-Electron. Phys.*, **11**, 03039 (2019).
10. S.Chattopadhyay, K.Neogi, A.Sarkar et al., *J. Magn.Mag.Mater.*, **323**, 363 (2011).
11. B.B.Straumal, A.A.Mazilkin, S.G.Protasova et al., *J.Phys.Rev.B*, **79**, 155203 (2009).
12. T.V.Manh, T.L.Phan, B.W.Lee et al., *IEEE Trans.Magn.*, **51**, 2400504 (2015).

13. V.Yu.Vorovsky, A.V.Kovalenko, A.I.Kushnerov et al., *J. Functional Materials*, **25**, 61 (2018).
14. O.V.Kovalenko, M.F.Bulaniy, V.Y.Vorovskiy et al., *J. Phys. Electr.*, **26**, 69 ( 2018).
15. S.C.Tsai, Y.L.Song, C.S.Tsai et al., *J. Mater. Sci.*, **39**, 3647 ( 2004).
16. A.S.Vorokh, *J. Nanosyst. Phys. Chem. Math.*, **9**, 364 (2018).
17. M.M.Mezdrogina, E.Yu.Danilovskiy, R.V.Kuzmin, *J. Semiconductors*, **44**, 321 (2010)).
18. O.Jayakumar, H.Salunke, R.Kadam et al., *J. Nanotechnology*, **17**, 1278 (2006).
19. D.Toloman, A.Mesaros, A.Popa et al., *J. Alloy. Compd.*, **551**, 502 (2013).
20. H.Zhou, D.M.Hofmann, A.Hofstaetter et al., *J. Appl. Phys.*, **94**, 1965 (2003).
21. A.Layek, G.Mishra, A.Sharma et al., *J. Phys. Chem. C*, **116**, 24757 (2012).
22. D.Ghica, I.D.Vlaicu, M.Stefan et al., *J. Sci. Rep.*, **9**, 6894 (2019).
23. E.V.Lavrov, F.Herklotz, J.Weber, *J. Phys. Rev.*, **79**, 165210 (2009).
24. D.M.Hoffmann, A.Hofstaetter, F.Leiter et al., *J. Phys. Rev. Lett.*, **88**, 045504-1 (2002)
25. C.Yanqiang, D.Wu, Q.Xu, *J. Appl. Surf. Sci.*, **271**, 421 (2013).
26. S.J.Guan, N.N.Asu, Yu.Zhang et al., *Sci. China Tech. Sci.*, 62 (2019).